Analysis of the chemical structure of a weakly unstable cellular gaseous detonation

Hiroaki Watanabe[1], Akiko Matsuo[2], Ashwin Chinnayya[1],
Noboru Itouyama[3], Ken Matsuoka[3], Jiro Kasahara[3]

[1]Institut Prime UPR 3346 CNRS, ISAE-ENSMA, Universite de Poitiers
1 avenue Clément Ader, BP 40109, 86961 Futuroscope-Chasseneuil CEDEX, France

[2]Keio University
3-14-1, Hiyoshi, Kohoku-ku, Yokohama, Kanagawa, 223-8522, Japan

[3]Nagoya University
Furo-cho, Chikusa, Nagoya, Aichi, 464-8603, Japan

1 Introduction

Detonation wave exhibits an unsteady and complex multi-dimensional cellular structure [1]. The coupling of the chemical reactions and the hydrodynamic instability is vital for the cellular detonation propagation. Previous studies revealed that the cellular structure got irregular for increased χ parameter and reduced activation energy, due to the interactions between gas dynamics and chemistry [2]. For lower isentropic coefficient, another mechanism came into play, during the triple point collision. Indeed, forward jets can interact with the Mach stem to develop another Mach stem, increasing also cell irregularity [3]. In addition, the geometry could also influence the regularity of the cellular structure, when the cell size becomes comparable to the characteristic length of the confinement [4, 5].

The mixture instability influences the ignition mechanism downstream of the leading shock front. In weakly unstable mixtures for which the reaction length is much longer than the induction length [6], the cellular structure is regular and the adiabatic compression of the leading shock front is the dominant mechanism for the ignition, which results in the good agreement of the dynamical behavior with the the steady ZND model. The transverse waves thus play a minor role in the propagation in regular cellular detonation [2]. On the other hand, the detonation in the unstable mixture has a irregular cellular structure. The discrepancy from the ZND model in the detonability limit becomes more apparent as the mixture instability increase [7]. Indeed, about 40% of the shocked gas can not ignite from the shock compression and the rest of the shocked gas are considered to be burnt by the turbulent flame behind the front in these mixtures [8]. Furthermore, the transverse waves contribute to the propagation of the detonation with irregular cell [2].

Lundstrom and Oppenheim [9] showed experimentally that the induction length became longer due to the unsteady expansion behind the leading shock. Dormal et al. [10] obtained the distribution of the induction time inside the cell by the emission spectroscopy of hydrooxyl radical and showed that the local induction time increased along the cell. Pintgen et al. [11] utilized the planar laser induced fluorescence technique to visualize the reaction front structure of detonation. They showed the nature of the disturbances in OH species induced by the variations in the strength of the leading shock front associated with the transverse wave instability of detonation. Later, Austin et al. [12] applied this methodology for the various mixture with different instabilities and found that the reaction front structure became more

complex as the reduced activation energy increased from the neutral stability curve. Besides, Hu et al. [13] numerically studied the structure in $H_2/O_2/Ar$ cellular detonation and found that a considerable region of the gas in a cell was ignited by the incident shock wave and transverse wave. Recently, Frederick et al. [14] analyzed the coupling of the leading shock front and the chemical reaction by a statistical analysis of the shock velocity and the induction length based on simultaneous schlieren and broadband chemiluminescence image. For stable mixtures, the joint pdf of the leading shock speed and the chemical length followed the trend by the quasi-steady model. Whereas for the unstable mixture, the pdf followed only the trend given by the quasi-steady model during the high-speed portion of the front.

Despite these aforementioned efforts, Eulerian point of view has a difficulty in tracking the history of gaseous particles to analyze the evolution of the chemical species and the thermodynamic properties, as Taylor et al. [15] pointed out. The Lagrangian point of view has a merit for this purpose. In some previous studies [16–20], the analysis using the Lagrangian particle tracking method was used and succeeded in getting insight behind the detonation front. However, the distribution of the induction time and reaction time inside the cellular structure from the Lagrangian point of view have yet to be discussed. To deepen our knowledge for the chemical structure of cellular gaseous detonation, the unsteady two-dimensional (2D) numerical simulations using the Lagrangian particle tracking method and the detailed chemistry have been conducted for one weakly unstable mixture.

2   Numerical setup and problem statement

The governing equations for the gaseous phase are the 2D reactive compressible Navier-Stokes equations, with the ideal equation of state. The chemical reaction mechanism proposed by Hong et al. [21], which considers 9 species (H_2, O_2, H, O, OH, H_2O, HO_2, H_2O_2 and Ar) and 20 elemental reaction, is used. The other numerical models and methods were the same as our previous study [22].

The trajectory of the massless Lagrangian particles are obtained by a Lagrangian particle tracking method. The position of the Lagrangian particles are updated using the gas velocity at the Lagrangian particle position. The time when the massless gaseous particles passed the leading shock front can thus be recorded, as well as for other variables such as maximum thermicity time.

The fully developed two-dimensional gaseous detonation propagated in the two-dimensional straight channel. 70% diluted stoichiometric hydrogen oxygen mixture $2\,H_2 - O_2 - 7\,Ar$ at ambient conditions (0.1 MPa and 300 K) was utilized as the target gas. The channel widths was 2.6 mm. The out flow boundary was applied to the left end. The grid was uniform and was equal at 2.0 μm from the region from the shock front up to 20.6 mm behind the front. Then, the grid was stretched. The grid resolution was about 38 points per the CJ induction length (x_{ind}) and this resolution was enough to reproduce the feature of the instantaneous flow field for weakly unstable mixtures [23]. The length of the propagation was about 1000 x_{ind} by the recycling block technique [24]. The average cell width in the simulation was estimated as 1.3 mm. The average propagation velocity agreed with the CJ velocity in the present conditions.

The massless gaseous particles were initially located in the fresh mixture in every grid point. The number of these particles inside the computational domain changed during the simulation due to the recycling block method and were around 34 millions. In order to obtain the reaction time for each Lagrangian particle, the same simulation was repeated two times. In the first simulation, the maximum thermicity value and its time for each Lagrangian particle were recorded to estimate the induction time. After the first simulation to record the maximum thermicity, the second simulation was conducted with the same initial conditions and numerical methods and the half pulse width of thermicity was recorded to obtain the reaction time. In this study, the induction time is defined as the time from the leading shock front passage to the time when the thermicity became maximum, and the reaction time is defined as the time within the half thermicity pulse width.
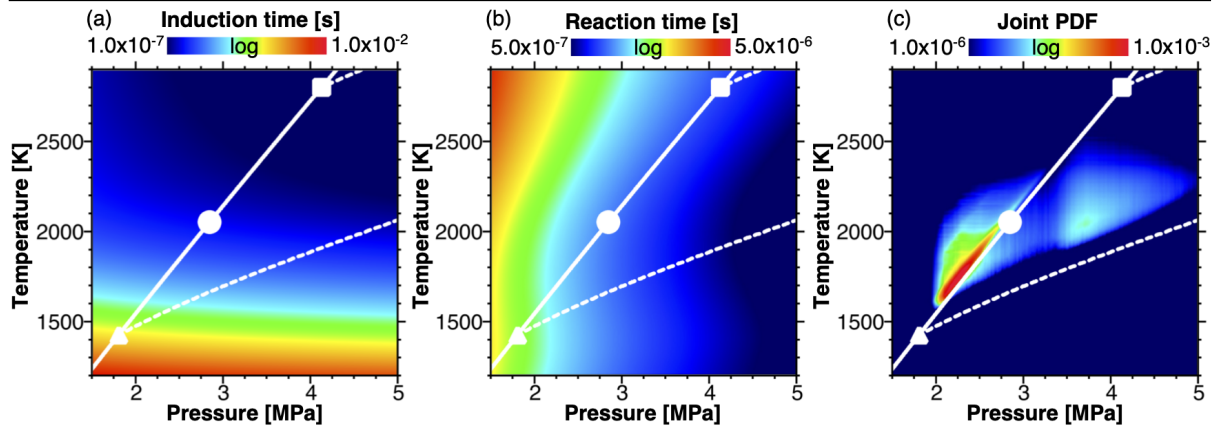
Figure 1: p-T diagram. (a) induction time from 0D constant volume simulation, (b) reaction time from 0D constant volume simulation, (c) Joint pdf for the unburned mixture behind the shock front in simulations. The unburned mixture whose H_2 mass fraction was higher than 0.1275 and slightly lower than its initial value was taken into account. The white solid line represents the state along the Rankine-Hugoniot line. The white broken line is the state behind the reflected shock wave. The white circle, triangle and square indicate the states for the von Neumann state at the CJ velocity, 0.8 CJ velocity and 1.2 CJ velocity, respectively.

3   Results and discussions

Figure 1 depicts the induction time, reaction time from 0D constant volume simulation and the joint pdf for the states of the unburned mixture from simulation results in p-T diagram to understand how the unburned mixture reacts and the chemical times are dependent on the thermodynamic state just behind the shock fronts. The induction time showed a strong temperature dependency and changed by orders of magnitude with respect to the initial temperature (Fig. 1(a)). In addition, the effect of initial pressure on induction time was less significant. On the other hand, the dependency of the reaction time with respect to the initial pressure was higher than that of the initial temperature (Fig. 1(b)). The state for the unburned mixture behind the front was mostly distributed along the Rankine-Hugoniot line below the CJ state (Fig. 1(c)). However, some portion of the unburned gas lay along the shocked gas from the Hugoniot curve, due to the transverse wave.

   The variations in the cells are shown in Fig. 2. Here, the transverse wave time was defined as the time from the leading shock passage to the time when the Lagrangian particle experienced the transverse wave. The front structure and the cell were regular in $2\,H_2-O_2-7\,Ar$ mixture (Figs. 2(a,b)) and the strong transverse wave structure occurred in the second part of the cell (Fig. 2(a)). The distributions of the induction time, the reaction time, and the transverse wave time were non uniform inside the cell (Figs. 2(c,d,f)). The first observation on the induction time was that the induction process finished within $1/2$ of the cell cycle (Fig. 2(c)). The second observation was that the main heat release occurred within $1/4$ of the cell cycle (Fig. 2(d)). The induction time did not monotonically increase along the cell as in Dormal et al. [10], who obtained it from an Eulerian point of view. The maximum induction time could be found around the center of the cell in its second part in our case. This discrepancy could be ascribed to the differences in the definition of the induction time. It was confirmed that the same trend as in Ref. [10] could be obtained if the same definition was used (not shown here). The distribution of the reaction time was also non uniform inside the cell, with a maximum around the center of the cell in the first part of the cell (Fig. 2(d)). The reaction time then decreased from the first to the second part of the cell, due to the transverse waves. The ratio of the induction time to the reaction time (Fig. 2(e)) was smaller than one in the first part of the cell and around the edges of the cell in its second part. This
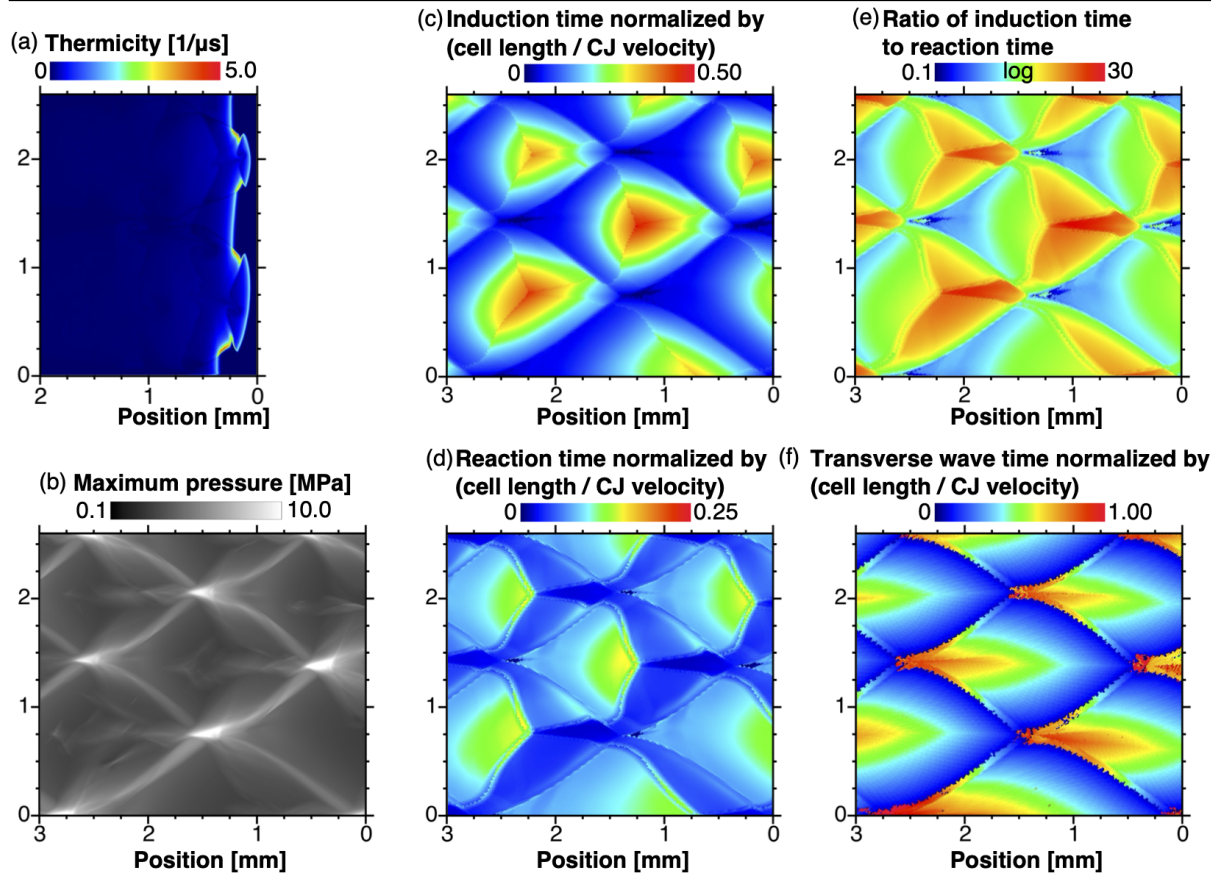
Figure 2: Variation in the cells. (a) Instantaneous 2D flow field for thermicity, (b) maximum pressure, (c) induction time τ_{ind} normalized by L/D_{CJ}, (d) reaction time τ_{reac} normalized by L/D_{CJ}, (e) ratio of induction time to reaction time $\tau_{\text{ind}}/\tau_{\text{reac}}$, (f) normalized transverse wave time $\tau_{\text{TW}}/(L/D_{\text{CJ}})$. The Lagrangian data are displayed in (c,d,e,f) in their initial position.

meant that power pulses originating from neighboring particles will overlap [2]. This ratio increased up to 30 locally due to much shorter reaction time in the regions where the collision of the transverse waves occurred. This is consistent with the analysis of Figs. 1(a,b). The Lagrangian particles experienced the transverse wave within one cell cycle (Fig. 2(f)). The transverse wave time were longer at the center line of the cell and particularly near the start of the cell cycle. On the other hand, near the edges of the cell in its second part, the Lagrangian particles experienced the transverse wave before approximately the CJ induction time.

The time sequence of the induction time is presented in Fig. 3. In the first part of the cell where the Lagrangian particles experienced the Mach stem, the induction time were shorter due to higher initial temperatures behind the leading shock (Figs. 3(a,b) and 1(a)). The ignition was induced by the adiabatic shock compression without the effect of the transverse wave (see Fig. 2(f)). In the second part of the cell near its edges, the Lagrangian particles experienced the transverse waves soon after the passage of the incident shock front, resulting in shorter induction time despite the lower initial temperature by the weak leading shock front (Figs. 3(c,d,e,f)). As for the Lagrangian particles initially located around the center of the cell in the second part of the cell, the induction process was enhanced by the transverse wave passage and after the collision of the triple points (Figs. 3(d,e,f)).

Although the transverse waves were considered to play the minor role in the propagation of the weakly unstable cellular detonation in the previous studies [2,6], the present results clearly showed that
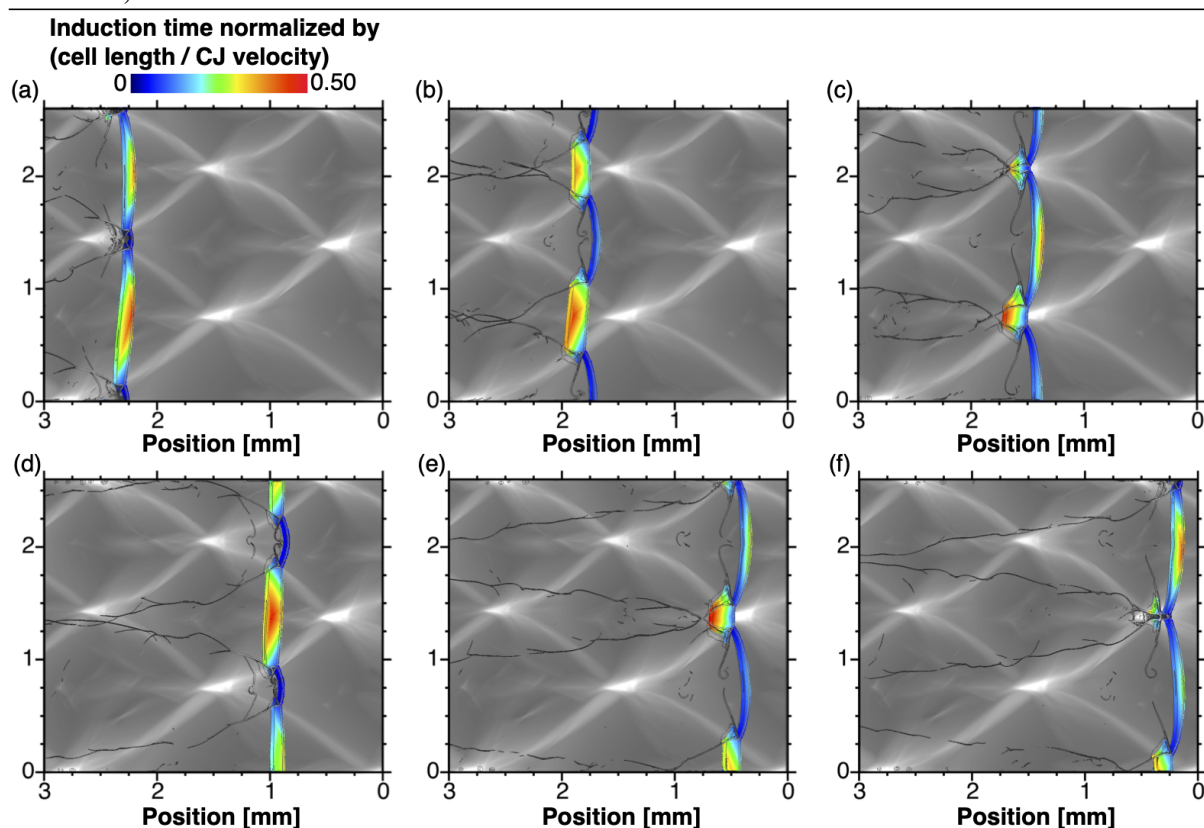
Figure 3: Time sequence of instantaneous 2D flow fields of the induction time. Only the Lagrangian particles whose time from shock front passage is less than the induction time are displayed. The lines are the density Schlieren and the gray contour in the background is the maximum pressure. The detonation propagated from the left to the right and the time passed from (a) to (f).

the transverse waves did contribute to enhance the chemical reactions, even in the weakly unstable case.

4 Conclusions

The chemical structure of a weakly unstable cellular gaseous detonation was studied by 2D numerical simulation with the Lagrangian particle tracking method. The distribution of the induction and reaction times inside the cell was obtained for the first time. Due to the decaying leading shock front and the transverse wave structure, the chemical times were non-uniform. The induction time became maximum around the center of the cell in its second part. The reaction time also became shorter in the second part of the cell due to higher initial pressure by the transverse wave. This may result in the incoherence of the power pulses from neighbor particles. The induction process completed within the half of the cell cycle and transverse waves played a key role in enhancing the chemical reaction even in the weakly unstable cellular detonation.

Acknowledgement

gram "Investissements d'Avenir" (EUR INTREE, reference ANR-18-EURE-0010). HW is supported by JSPS Overseas Research Fellowships.

References

[1] Lee JHS. (2008). The detonation phenomenon. Cambridge University Press.

[2] Radulescu MI., The propagation and failure mechanism of gaseous detonations: experiments in porous-walled tube, Ph.D. diss., McGill University, 2003.

[3] Sow A., Lau-Chapdelaine SM., Radulescu MI. (2021). The effect of the polytropic index γ on the structure of gaseous detonations. Proc. Combust. Inst. 38: 3633.

[4] Monnier V., Rodriguez V., Vidal P., Zitoun R. (2022). An analysis of three-dimensional patterns of experimental detonation cells. Combust. Flame 245: 112310.

[5] Crane J., Lipkowicz J. T., Shi X., Wlokas I. Kempf A. M., Wang H. (2022). Three-dimensional detonation structure and its response to confinement. Proc. Combust. Inst. 39: 1.

[6] Xiao Q., Radulescu MI. (2020). Dynamics of hydrogen-oxygen-argon cellular detonations with a constant mean lateral strain rate. Combust. Flame 215: 437.

[7] Xiao Q., Radulescu MI. (2020). Role of instability on the limits of laterally strained detonation waves. Combust. Flame 220: 410.

[8] Kiyanda CB., Higgins AJ. (2013). Photographic investigation into the mechanism of combustion in irregular detonation waves. Shock Waves 23: 115.

[9] Lundstrom EA., Oppenheim AK. (1969). On the influence of non-steadiness on the thickness of the detonation wave. Proc. Roy. Soc. A. 310: 463.

[10] Dormal M., Libouton JC., Tiggelen PJV. (1979). Evolution of induction time in detonation cells. Acta Astronaut. 6: 875.

[11] Pintgen F., Eckett CA., Austin JM., Shepherd JE. (2003). Direct observation of reaction zone structure in propagating detonations. Combust. Flame 133: 211.

[12] Austin JM., Pintgen F., Shepherd. JE. (2005). Reaction zones in highly unstable detonations. Proc. Combust. Inst. 30: 1849.

[13] Hu XY., Zhang DL., Khoo BC., Jiang ZL. (2004). The structure and evolution of a two-dimensional H2/O2/Ar cellular detonation. Shock Waves 14: 37.

[14] Frederick MD., Gejji RM., Shepherd JE., Slabaugh CD. (2022). Statistical analysis of detonation wave structure. Proc. Combust. Inst. 39: 1.

[15] Taylor BD., Kessler DA., Gamezo VN., Oran ES. (2013). Numerical simulations of hydrogen detonations with detailed chemical kinetics. Proc. Combust. Inst. 34: 2009.

[16] Eckett CA., Quirk JJ., Shepherd JE. (2000). The role of unsteadiness in direct initiation of gaseous detonations. J. Fluid Mech. 421: 147.

[17] Arienti M., Shepherd JE. (2005). A numerical study of detonation diffraction. J. Fluid Mech. 529: 117.

[18] Shi L., Uy KCK., Wen CY. (2020). The re-initiation mechanism of detonation diffraction in a weakly unstable gaseous mixture. J. Fluid Mech. 895: A27.

[19] Kozak Y., Dammati SS., Bravo LG., Hamlington PE., Poludnenko AY. (2020). WENO interpolation for Lagrangian particles in highly compressible flow regimes. J. Comput. Phys. 402: 109054.

[20] Brouzet D., Vignat G., Ihme M. (2022). Dynamics and structure of detonations in stratified product-gas diluted mixtures. Proc. Combust. Inst. 39: 1.

[21] Hong Z., Davidson DF., Hanson RK. (2012). An improved H2/O2 mechanism based on recent shock tube/laser absorption measurements. Combust. Flame 158: 633.

[22] Watanabe H., Matsuo A., Chinnayya A., Matsuoka K., Kawasaki A., Kasahara J. (2020). Numerical analysis of the mean structure of gaseous detonation with dilute water spray. J. Fluid Mech. 887: A4.

[23] Mazaheri K., Mahmoudi Y., Radulescu MI. (2012) Diffusion and hydrodynamic instabilities in gaseous detonations. Combust. Flame 159: 2138.

[24] Sow A., Chinnayya A., Hadjadj A. (2019). On the viscous boundary layer of weakly unstable detonations in narrow channels. Comput. Fluids 179: 449.